PCCP

PAPER

View Article Online
View Journal | View Issue

Cite this: *Phys. Chem. Chem. Phys.*, 2018, **20**, 25217

Superconductivity and phase stability of potassium-doped biphenyl†

Guo-Hua Zhong,[a] Dong-Yu Yang,[b] Kai Zhang,[b] Ren-Shu Wang,[b] Chao Zhang,[c] Hai-Qing Lin*[d] and Xiao-Jia Chen*[b]

Received 14th August 2018,
Accepted 6th September 2018

DOI: 10.1039/c8cp05184d

rsc.li/pccp

Phenyl molecules are proposed as potential high-temperature superconductors due to exhibiting interesting properties. Here, we report the discovery of superconductivity with the critical temperature (T_c) of ~7.2 Kelvin in potassium (K)-doped biphenyl ($C_{12}H_{10}$). The dc magnetic susceptibility measurements provide solid evidence for the presence of the Meissner effect in $K_xC_{12}H_{10}$. The Raman spectra detected bipolaronic characteristics in this superconducting state, which are proposed to account for the electron pairing. Theoretical simulations provided the information of the crystal structure of $K_xC_{12}H_{10}$. Combining XRD data with formation energy, we suggest that the superconducting phase corresponds to $K_2C_{12}H_{10}$ or with a small charge fluctuation in a layered structure. The discovery of superconductivity in K-doped biphenyl vastly expands the potential applications in the superconducting field.

1 Introduction

Organic materials have attracted increasing interest because of their many fascinating phenomena such as low dimensionality, strong electron–electron and electron–phonon interactions and the proximity of antiferromagnetism, insulator states and superconductivity. Especially, organic based compounds were suggested as candidates for high temperature or room temperature superconductors since the electrons can interact with much higher excitation energy than the phonon energy in these materials.[1,2] Numerous studies have been done over a half century. In 1965, the first carbon-based superconductor C_8A (A represents the alkali metal) was studied, exhibiting a superconducting transition temperature (T_c) of 0.02–0.55 K.[3] In 2005, the T_c values of graphite-like superconductors were raised to 6.5 and 11.5 K for YbC_6 and CaC_6, respectively.[4,5] In 1991, superconductivity was also observed in the complete carbon material of fullerene by doping potassium (K), with T_c ~ 18 K.[6] Furthermore, the T_c in cesium-doped fullerene reached to 38 K.[7] In 1980, a real organic superconductor consisting of C and H atoms, di-(tetramethyltetraselenafulvalene)-hexauorophosphate, named $(TMTSF)_2PF_6$, was reported with T_c equaling 0.9 K under 1.2 GPa.[8] Then, in 2003, the T_c was raised to 13.4 K in the BEDT-TTF salt family under 8.2 GPa.[9] Recently, an interesting superconductivity has been discovered in polycyclic aromatic hydrocarbons (PAHs) doped by alkali metals.[10–15] The PAH materials exhibit the characteristics of multi-T_c phases and the highest value of T_c increases with the number of benzene rings, reaching 33 K in K-doped 1,2:8,9-dibenzopentacene.[13] In addition, researchers observed that the poly(*para*-phenylene) (PPP) materials, such as K-doped *p*-terphenyl,[16–20] *p*-quaterphenyl,[21,22] and *p*-quinquephenyl,[23] which are non-edge-shared aromatic hydrocarbons, also possess rich superconductivities. It is worth mentioning that *p*-terphenyl was found to be superconducting with T_c as high as 123 K,[19] which is comparable to the record high T_c of about 130 K in some cuprate superconductors at ambient pressure.[24] This discovery of high T_c superconductivity in *p*-terphenyl seemingly supports the above idea suggested by Little and Ginzburg.

Interestingly, the low-T_c phase with T_c in the range of 5–7 K exists in observed PAH superconductors,[10–15] though some PAHs exhibit the characteristics of multi-T_c phases. By exploring the superconductivity of K-doped solid benzene, which is a basic unit of aromatic compounds (the electron–phonon coupling constant λ = 0.67 and T_c = 6.2 K), theoretical studies pointed out that the low T_c phase of 5–7 K is a common feature for all aromatic hydrocarbon superconductors and is easy to obtain due to better stability.[25] The subsequent experimental investigations confirmed the observation, for example, 7.2 K in *p*-terphenyl[17] and *p*-quaterphenyl,[22] 7.3 K in *p*-quinquephenyl,[23] 7.2 K in 2,2′-bipyridine,[26] and 3.5/7.2 K in triphenylbismuth.[27] The π electron network plays an important role in the superconductivity of PAH and PPP compounds and drives a strong

[a] *Shenzhen Institutes of Advanced Technology, Chinese Academy of Sciences, Shenzhen 518055, China*
[b] *Center for High Pressure Science and Technology Advanced Research, Shanghai 201203, China. E-mail: xjchen@hpstar.ac.cn*
[c] *Department of Physics, Yantai University, Yantai, 264005, China*
[d] *Beijing Computational Science Research Center, Beijing, 100193, China. E-mail: haiqing0@csrc.ac.cn*

† Electronic supplementary information (ESI) available: Atomic coordinates and bond lengths for pristine and doped biphenyl. See DOI: 10.1039/c8cp05184d

coupling of the charge carriers to the lattices. The electron–phonon interactions can account for the superconductivity of this unified superconducting phase.[25,28] Within the framework of BCS theory, an increase of doping concentration may result in a stronger electron–phonon interaction, which is helpful for obtaining a higher T_c,[29] and the pressure can also drive a higher T_c.[30]

However, the electron–phonon interaction is not enough to produce the high T_c superconductivity such as 18 K in picene,[10] 15 K in coronene,[11] 33 K in 1,2:8,9-dibenzopentacene,[13] and 43/123 K in *p*-terphenyl.[18] Other factors may play important roles in the high T_c superconductivity. Key features of organic superconductors are the low dimensionality of the materials and strong electron–electron correlation. The fulleride Cs_3C_{60} was found to be a true Mott insulator because of strong electronic correlation effects,[31] though it could be turned into a superconductor by pressure.[7] Superconductivity induced by pressure in Cs_3C_{60} was found to be related to the antiferromagnetic Mott insulator.[32] K_3 picene was also revealed as a strongly correlated electron system,[33,34] which results in the absence of metallicity.[35] Theoretical calculations predicted that K-doped PAHs in their ground state exhibit near antiferromagnetic behaviour.[34,36,37] Especially for K-doped *p*-terphenyl, the bipolaronic characteristic has been identified from Raman scattering measurements.[17–19] Photoemission spectroscopy conducted on surface K-doped *p*-terphenyl crystals showed a gap persisting up to at least 120 K that shares a similar temperature dependence to the obtained spectra of Bi–Sr–Ca–Cu–O superconductors.[38] Furthermore, an analogous gap below 50 K was also found in K-doped *p*-terphenyl films fabricated on Au(111).[39] All these features indicate that the high T_c superconductivity of organic materials with π-electron networks cannot simply be explained by the electron–phonon mechanism. This indicates that both the electron–phonon interaction and electron–electron correlations work together to enhance the T_c of aromatic hydrocarbons with increasings numbers of benzene rings.[25]

Due to the appearance of superconductivity and possible high T_c, PPP superconductors provide a good system to study the interplay of strong electron–electron and electron–phonon interactions in a low-dimensional system. Comparing with *p*-terphenyl, biphenyl ($C_{12}H_{10}$) is the shortest polymer with only two phenyl rings connected by a single C–C bond. It shows a relatively simple monoclinic structure, and it undergoes an incommensurate triclinic transition at about 40 K.[40] In this work, therefore, we have synthesizedK-doped biphenyl ($K_xC_{12}H_{10}$) and observed the Meissner effect in this material. The dc magnetic measurements support the existence of superconductivity with $T_c \sim 7.2$ K in this material. Combining with the first-principles calculations, we predicted the crystal structure and electronic band feature of this superconducting phase to understand the superconductivity of K-doped biphenyl. Our results report the smallest *p*-oligophenyl superconductor and present the possible microstructure.

2 Experimental and computational methods

2.1 Experimental details

High quality potassium and crystalline biphenyl were purchased from Sinopharm Chemical Reagent and Alfa Aesar, respectively. In our experiments, the doped biphenyl was synthetized by heating a mixture of small pieces of fresh potassium and biphenyl with a mole ratio of 3 : 1 at a temperature of 120°–130 °C for 48 hours. All the synthesis procedures were performed in a glove box with moisture and oxygen levels less than 0.1 ppm, and the sample was sealed in a quartz tube under a high vacuum of better than 1×10^{-4} Pa in the heating process. The dc magnetization measurements were performed in the temperature range from 1.8 K to 300 K by a commercial Magnetic Property Measurement System (Quantum Design). In the Raman scattering experiments, a 660 nm excitation was applied to obtain the Raman spectra of the pristine and doped biphenyl. The laser power was selected as less than 2 mW before a ×20 objective to avoid possible damage of samples. The X-ray diffraction experiments were performed in the 2-theta range of 5°–60° by an X-ray diffractometer (Empyrean, PANalytical B.V.). The samples were put on specific glasses and then covered with thin films to isolate the air.

2.2 Computational details

To study the structural and electronic properties of pristine and K-doped biphenyl, we employed the Vienna ab initio simulation package (VASP)[41,42] based on the projector augmented wave method. For the planewave basis-set expansion, an energy cutoff of 600 eV was adopted. The Monkhorst–Pack *k*-point grids were generated according to the specified *k*-point separation of 0.02 $Å^{-1}$ and the convergence thresholds were set as 10^{-6} eV in energy and 10^{-3} eV $Å^{-1}$ in force. The generalized gradient form (GGA) of the exchange–correlation functional (Perdew–Burke–Ernzerh of 96, PBE) was adopted.[43] Considering the non-local interactions, we added the correction of van der Waals (vdW) in the version of vdW-DF2 in the calculations.[44] The necessity of the vdW-DF2 functional has been confirmed by our previous studies.[29,45]

3 Results and discussion

3.1 Meissner effect

The Meissner effect and zero resistivity are two fundamental features of superconductivity. Actually, metal-doped carbon-based superconductors were mainly detected from magnetic measurement.[10–15] However, with its small diamagnetic volume and easily damaged crystal structure, the metallic state of $K_xC_{12}H_{10}$ was hard to realize even below T_c. Difficulties in detecting weak superconductivity from resistivity measurements can be overcome by using magnetic susceptibility experiments. Hence, the superconductivity of $K_xC_{12}H_{10}$ was mainly characterized by magnetization measurements.

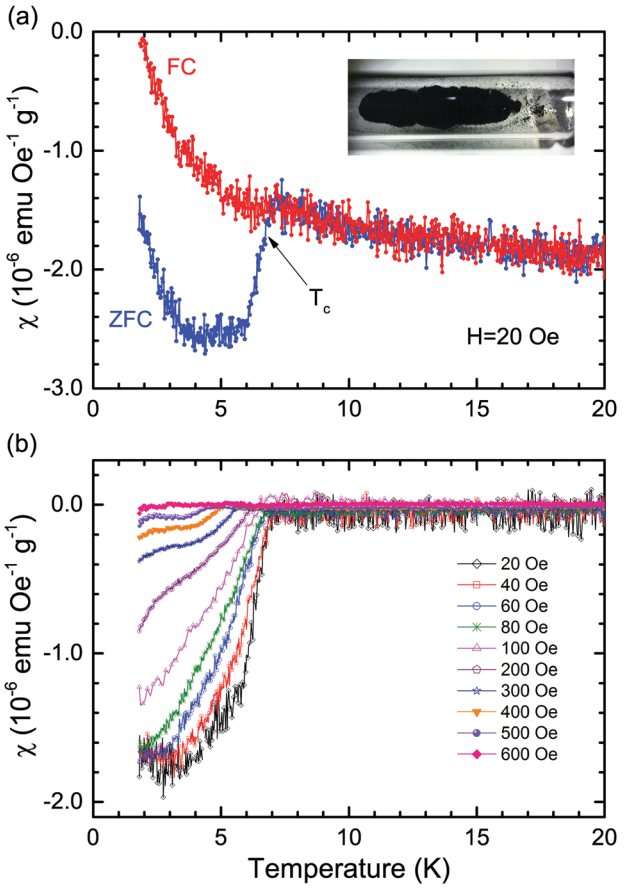

Fig. 1 (a) The temperature dependence of dc magnetic susceptibility χ for K_x biphenyl in the applied magnetic field of 20 Oe with field-cooling (FC) and zero-field cooling (ZFC). Inset is the black synthetic sample of K_x biphenyl. (b) The temperature dependence of χ for K_x biphenyl measured at various magnetic fields up to 600 Oe in the ZFC run.

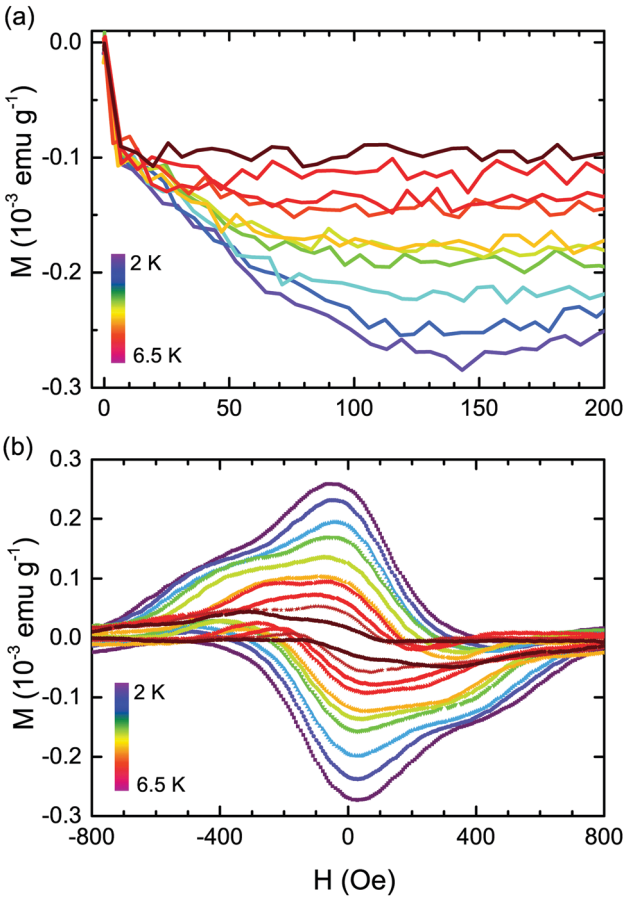

Fig. 2 (a) The magnetic field dependence of magnetization for K_x biphenyl at various temperatures in the superconducting state. (b) The magnetization hysteresis loop with scanning magnetic field along two opposite directions up to 800 Oe measured at various temperatures in the superconducting state.

Fig. 1(a) shows the dc magnetic susceptibility χ of the powder sample $K_xC_{12}H_{10}$ [inset of Fig. 1(a)] *versus* temperature measured in the zero-field cooling (ZFC) and field cooling (FC) cycles at 20 Oe. We can see a sudden drop of χ at the temperature of 7.2 K in the ZFC run, indicating that a superconducting transition occurs in this sample $K_xC_{12}H_{10}$. The superconducting transition temperature T_c was determined as 7.2 K. Supposing that the density ρ of this sample is about 3 g cm^{-3}, we can obtain the shielding fraction $4\pi\chi\rho$ = 0.004% from Fig. 1(a). Such a small shielding fraction is due to the existence of impurities and the smaller size of crystallites compared to the London penetration depth in this powder sample. Noticeably, both ZFC and FC χ show an upturn trend at a lower temperature than T_c, which implies a strong paramagnetic signal. The magnetic susceptibility of $K_xC_{12}H_{10}$ as a function of temperature in the ZFC run under different magnetic fields was also obtained to demonstrate the superconducting transition of $K_xC_{12}H_{10}$. As shown in Fig. 1(b), the diamagnetism of $K_xC_{12}H_{10}$ gradually decreases with increasing magnetic field. That is, the superconducting transition gradually disappears with increasing magnetic field since it is suppressed by the applied magnetic field. However, the superconductivity can be observed until the magnetic field is larger than 500 Oe.

The magnetic field dependence of the magnetization for the superconducting $K_xC_{12}H_{10}$ at various temperatures from 2 K to 6.5 K with low applied fields is summarized in Fig. 2(a). The linear behavior of the magnetic-dependent magnetization signals the Meissner effect in this superconductor. The superconductivity is suppressed as the temperature increases above 7 K. Fig. 2(b) shows the magnetization hysteresis loop with magnetic field along two opposite directions up to 800 Oe at various temperatures from 2 K to 6.5 K in this superconducting state. The symmetric hysteresis loops indicate that this sample exhibits a strong bulk pinning, which is certification of a type II superconductor.

3.2 Raman spectra

To understand this superconducting material from the aspect of the molecular dynamics process, we measured the Raman scattering spectra of the pristine and the doped biphenyl by using a laser wavelength of 660 nm, respectively shown in Fig. 3. According to previous studies,[26,46,47] all of the major peaks in the spectra of pristine biphenyl can be assigned and classified as the ring deformation, ring breathing, C–H bending, and C–C

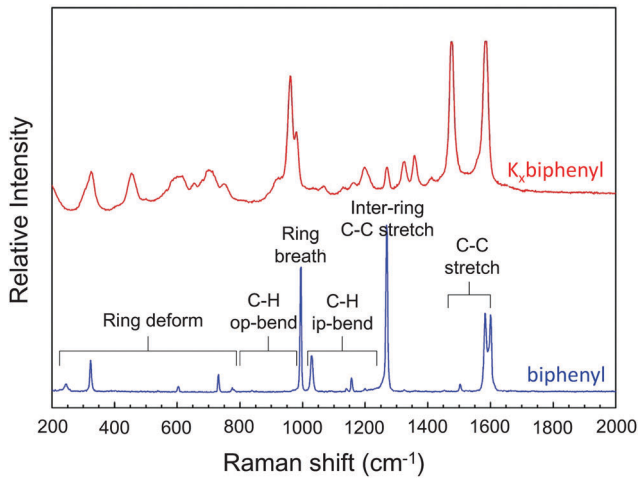

Fig. 3 Raman spectra of the doped (upper) and pristine (bottom) biphenyl excited by a laser wavelength of 660 nm.

stretching. The peaks in the range of 200–800 cm^{-1} mainly come from the the ring deformation. The bands from 800 to 1000 cm^{-1} and from 1000 to 1250 cm^{-1} were formed by the C–H bending out-plane and the C–H bending in-plane, respectively. The two peaks near 1000 and 1250 cm^{-1} arise from the ring breathing and the inter-ring C–C stretching, respectively. The peaks around 1600 cm^{-1} are due to the intra-ring C–C stretching.

It is well-known that polarons and bipolarons are able to form in conducting polymers.[48] Moreover, bipolaronic characterization in alkali-metal doped PPPs synthesized by different methods has been extensively studied in previous works.[49,50] The almost separated two intra-ring C–C stretching modes at around 1595 cm^{-1} in the spectra of pristine biphenyl downshift and merge with bipolaronic bands localized at 1586 cm^{-1}. The observation of the 1475 cm^{-1} mode with no corresponding band in the parent sample can be considered as the fingerprint for the formation of bipolarons. The 1325 cm^{-1} and 1360 cm^{-1} bands of $K_xC_{12}H_{10}$ originate from the inter-ring C–C stretching mode at 1265 cm^{-1} of the pristine sample. The upshifts in wavenumber reflect the decrease of length in the C–C bonds between rings. The 1260 cm^{-1} mode present in the Raman spectra of $K_xC_{12}H_{10}$ is due to the C–H bending in-plane, corresponding to the 1200 cm^{-1} mode in the pristine sample. The two bipolaronic bands at 1160 and 1200 cm^{-1} are induced by the C–H bending in-plane, corresponding to the 1155 cm^{-1} mode in the pristine sample. The bands localized at 965 cm^{-1} are from the C–H bending out-plane. These bands also exhibit bipolaronic characteristics. As a result, the Raman characterization of $K_xC_{12}H_{10}$ proves the existence of bipolarons, which possibly accounts for the observed superconductivity in $K_xC_{12}H_{10}$.

3.3 Crystal structure and stability

The identification of crystal structure and the investigation of electronic properties are helpful for exploring this superconductor. Therefore, we carried out first-principles calculations

Table 1 Optimized crystal parameters of $C_{12}H_{10}$ and $K_xC_{12}H_{10}$, including the space-group, the lattice constants, the angle, and the volume of unit cell

System	Space-group	a (Å)	b (Å)	c (Å)	α (°)	β (°)	γ (°)	V (Å^3)
$C_{12}H_{10}$[50]	$P2_1/c$	11.763	5.580	7.820	90	126.9	90	410.6
$C_{12}H_{10}$	$P2_1/c$	11.862	5.532	7.965	90	127.6	90	414.0
$K_1C_{12}H_{10}$	$P2_1$	7.193	7.142	9.411	90	104.0	90	469.1
$K_{1.5}C_{12}H_{10}$	$P1$	9.218	8.792	12.158	88.0	148.4	92.4	516.4
$K_2C_{12}H_{10}$	$P2_1/c$	11.445	5.473	10.468	90	123.0	90	550.1
$K_3C_{12}H_{10}$	$P2_1/c$	12.755	6.099	9.032	90	102.5	90	686.1

to predict the crystal and electronic structures of K-doped biphenyl. First, we performed a test in the case of the pristine sample. As shown in Table 1, we obtained the optimized crystal parameters of a = 11.862 Å, b = 5.580 Å, c = 7.965 Å, β = 127.6°, and V = 414.0 Å^3, which are in good agreement with the experimental values.[51] The result implies the feasibility of the theoretical study. Then, we considered four possible doping concentrations, x = 1, 1.5, 2, and 3 in $K_xC_{12}H_{10}$. Selecting the structures with the lowest total energy for each doping level, the optimized crystal parameters are summarized in Table 1 and the geometrical configurations are shown in Fig. 4. Detailed atomic coordinates and bond lengths for pristine and K-doped biphenyl stable structures are presented in the ESI† (Tables S1–S5 and Fig. S1–S5). After doping K metal into biphenyl, great changes took place in the lattice constants, and the volume of the unit cell gradually increased with the doping content. As shown in Fig. 4, the biphenyl molecules respectively form the herringbone configuration in $K_1C_{12}H_{10}$, $K_{1.5}C_{12}H_{10}$, and $K_3C_{12}H_{10}$ similar to K-doped PAHs,[10–15] however, a typical layered structure is observed in $K_2C_{12}H_{10}$. Noticeably, there is a tilted angle between two successive benzene rings in $K_1C_{12}H_{10}$, but this tilted angle disappears when increasing the K content. Viewing perpendicular to the molecular surface, the two ends of the biphenyl molecule are favorable for K atoms.

To examine the possible doping situation corresponding to our experiment, we analyzed the thermodynamic stability of these considered doping cases by calculating the formation energy E_f. In this work, the E_f for the doping level x is defined as a function of K chemical potential with the fomula

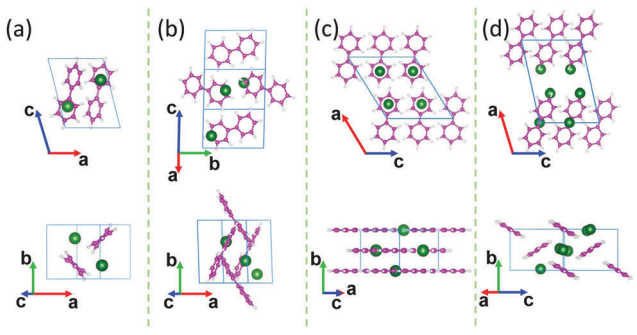

Fig. 4 Optimized crystal structures of $K_xC_{12}H_{10}$ viewed from different directions. (a–d) Correspond to $K_1C_{12}H_{10}$, $K_{1.5}C_{12}H_{10}$, $K_2C_{12}H_{10}$, and $K_3C_{12}H_{10}$, respectively. Red, gray, and green balls represent the C, H, and K atoms, respectively.

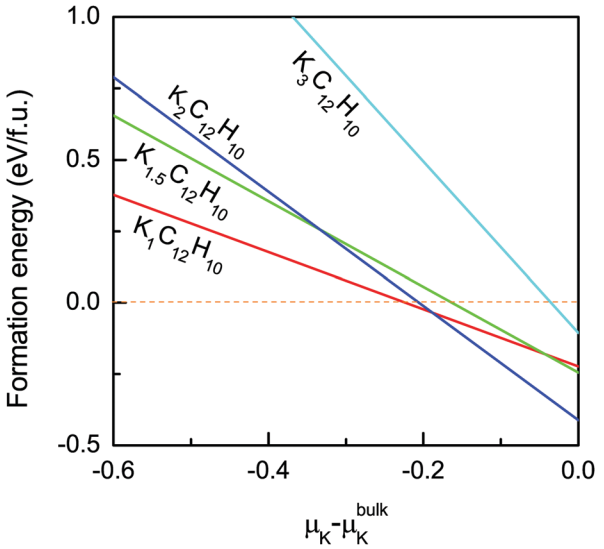

Fig. 5 Calculated formation energy of $K_xC_{12}H_{10}$ as a function of the K chemical potential.

$$E_f = E_{doped} - E_{pristine} - x\mu_K^{bulk} - x[\mu_K - \mu_K^{bulk}] \quad (1)$$

where E_{doped} and $E_{pristine}$ are the total energy of the doped and host crystal, respectively, μ_K^{bulk} can be obtained from the energy per K atom in the K metal with the bcc structure, x is the doping concentration, and μ_K is the chemical potential of the K species. Here $\mu_K = \mu_K^{bulk}$ means that the element is so rich that the pure element phase can form. $E_f < 0$ indicates that the doped compound can stably exist. From the calculated formation energy shown in Fig. 5, all of the considered doped phases are able to exist when the chemical potential of K satisfies a certain condition. Comparing several doping levels, however, $K_2C_{12}H_{10}$ is more stable since it has a lower formation energy than the other phases in a wide range of chemical potential because of the $E_f < 0$ condition. This suggests that the experimentally observed superconducting phase of 7.2 K is possibly $K_2C_{12}H_{10}$.

3.4 X-ray diffraction pattern

The X-ray diffraction (XRD) patterns shown in Fig. 6 further follow the superconducting state observed by experiment corresponding to the doping level of $x \sim 2$. Comparing the XRD spectra of the pristine and doped biphenyl from experiments, the (100) peak at 9° remains in K-doped biphenyl, which indicates that no big change exists in the lattice constant of a after doping. A new XRD peak marked as $(10\bar{2})$ appears at about 16° for this experimentally doped sample that is different from the pristine biphenyl, which means that there is an expansion of lattice constants along the c direction. Based on these constraints, we first checked the XRD patterns of the predicted structures of $K_1C_{12}H_{10}$, $K_{1.5}C_{12}H_{10}$, $K_2C_{12}H_{10}$, and $K_3C_{12}H_{10}$ shown in Fig. 6. It was found that several new XRD peaks emerge in the range of 10°–16° and the peak at 9° shifts towards to a higher angle in the two kinds of doping situations of $K_1C_{12}H_{10}$ and $K_{1.5}C_{12}H_{10}$. Moreover, the peak at 9° greatly

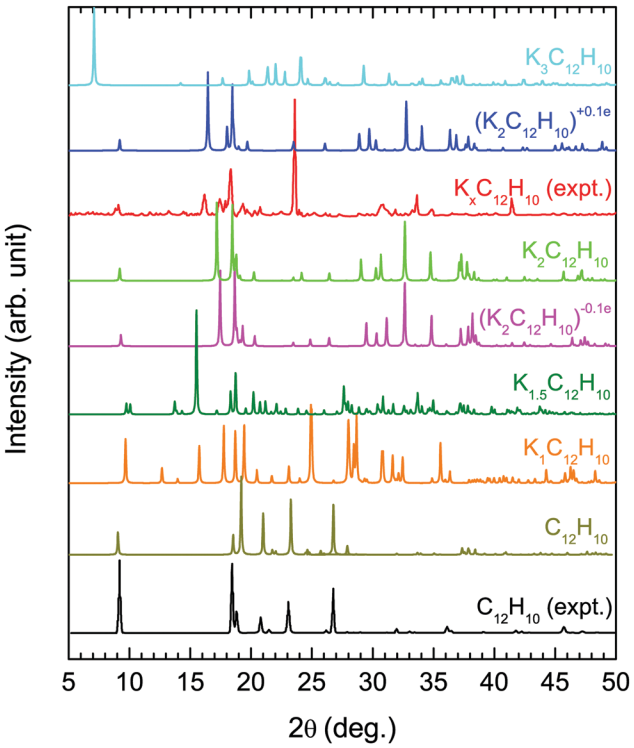

Fig. 6 Comparison of X-ray diffraction patterns of the pristine and doped biphenyl between experiments and theoretical calculations. $(K_2C_{12}H_{10})^{+0.1e}$ and $(K_2C_{12}H_{10})^{-0.1e}$ imply the injection and removal of a small number of electrons for $K_2C_{12}H_{10}$.

shifts towards a lower angle in $K_3C_{12}H_{10}$. Thus, we can exclude the possibility of $K_1C_{12}H_{10}$, $K_{1.5}C_{12}H_{10}$, and $K_3C_{12}H_{10}$ from the XRD patterns. Especially, $K_1C_{12}H_{10}$ exhibits antiferromagnetism instead of superconductivity.[52] Both $K_{1.5}C_{12}H_{10}$ and $K_3C_{12}H_{10}$ possess a higher formation energy, as shown in Fig. 5. The structure of $K_2C_{12}H_{10}$ produces XRD peaks near to those of the experimentally doped sample. As shown in Fig. 6, $K_2C_{12}H_{10}$ with a small fluctuating charge such as $(K_2C_{12}H_{10})^{+0.1e}$ (injected electron) exhibits coincident XRD peaks with the experimental sample, especially the peaks at low angles. Moreover, our previous studies demonstrated the stability and feasibility of doped PAHs with small charge.[45] Therefore, we can conclude that the observed superconducting state corresponds to $K_2C_{12}H_{10}$ or with a small fluctuated charge. The crystal structure of this superconducting material is shown in Fig. 4(c).

3.5 Electronic structures

Fig. 7(a) shows the band structure of $K_2C_{12}H_{10}$ along the high-symmetry k-points $\Gamma(0, 0, 0)$, $B(0.5, 0, 0)$, $A(0.5, 0.5, 0)$, $Y(0, 0.5, 0)$, $Z(0, 0, 0.5)$, $D(0.5, 0, 0.5)$, $E(0.5, 0.5, 0.5)$, and $C(0, 0.5, 0.5)$ in the Brillouin zone. Fig. 7(b) shows the total density of states (DOS) and projected density of states (PDOS) of $K_2C_{12}H_{10}$, $(K_2C_{12}H_{10})^{+0.1e}$ and $(K_2C_{12}H_{10})^{-0.1e}$. There is an indirect overlap between conduction bands and valence bands at the Fermi level of $K_2C_{12}H_{10}$ shown in Fig. 7(a), which means a small amount of electronic states [0.47 states per eV per f.u. shown in Fig. 7(b)] at the Fermi level. The density of states at the Fermi level is less than 4.6 states

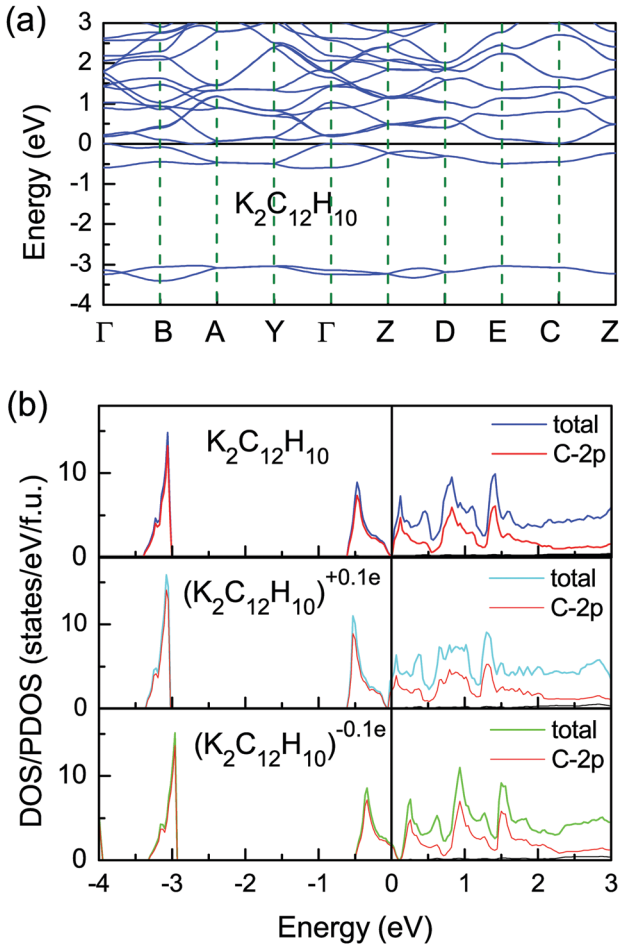

Fig. 7 The band structure of $K_2C_{12}H_{10}$ (a) and the DOS/PDOS of $K_2C_{12}H_{10}$, $(K_2C_{12}H_{10})^{+0.1e}$ and $(K_2C_{12}H_{10})^{-0.1e}$ (b). Zero energy denotes the Fermi level.

per eV per f.u. of $K_2C_6H_6$ where the T_c was predicted as 6.2 K.[25] Thus, based on the electron–phonon coupling mechanism, the predicted superconducting transition temperature T_c of $K_2C_{12}H_{10}$ is low. However, with a small fluctuated charge such as $(K_2C_{12}H_{10})^{+0.1e}$, the density of states at the Fermi level will increase to 3.4 states per eV per f.u. as shown in Fig. 7(b). There will be a big value for more additional charge. Additionally, from the PDOS shown in Fig. 7(b), we observe that the electronic states near the Fermi level are mainly contributed by the C 2p state, which means that the C atoms dominate the superconductivity of K-doped biphenyl.

4 Conclusions

In summary, we have synthesized K-doped biphenyl and carried out the magnetic susceptibility and Raman scattering measurements. Based on the Meissner effect, we found that K-doped biphenyl is superconducting with a T_c of 7.2 K. From the Raman spectra, the bipolaronic characteristics could be observed in this superconducting sample, which are proposed to account for the electron pairing. Furthermore, the crystal structure of this superconducting phase was suggested by employing first-principles calculations. Combining XRD data with formation energy, we suggested that the superconducting phase corresponds to $K_2C_{12}H_{10}$ or with a small charge fluctuation in a layered structure. Electronic states demonstrate the reasonability of the superconductivity of $T_c \sim 7$ K. The discovery of the superconductivity in K-doped biphenyl is an interesting and significant achievement in organic materials research. This discovery vastly expands the potential applications of superconducting materials.

Conflicts of interest

There are no conflicts to declare.

Acknowledgements

The work was supported by the National Natural Science Foundation of China (Grant No. 61574157 and 61774164) and the Basic Research Program of Shenzhen (Grant No. JCYJ20170818153404696 and JCYJ20150925163313898). We also acknowledge financial support from NSAF U1530401 and computational resources from the Beijing Computational Science Research Center. The calculation was partially supported by the Special Program for Applied Research on Super Computation of the NSFC-Guangdong Joint Fund (the second phase) under Grant No. U1501501. Experiments at HPSTAR were supported by the National Key R&D Program of China (Grant No. 2018YFA0305900).

Notes and references

1 W. A. Little, *Phys. Rev.*, 1964, **134**, A1416–A1424.
2 V. L. Ginzburg, *Sov. Phys. Usp.*, 1976, **19**, 174–179.
3 N. B. Hannay, T. H. Geballe, B. T. Matthias, K. Andres, P. Schmidt and D. MacNair, *Phys. Rev. Lett.*, 1965, **14**, 225–226.
4 T. E. Weller, M. Ellerby, S. S. Saxena, R. P. Smith and N. T. Skipper, *Nat. Phys.*, 2005, **1**, 39–41.
5 N. Emery, C. Hérold, M. d'Astuto, V. Garcia, C. Bellin, J. F. Marêché, P. Lagrange and G. Loupias, *Phys. Rev. Lett.*, 2005, **95**, 087003.
6 A. F. Hebard, M. J. Rosseinsky, R. C. Haddon, D. W. Murphy, S. H. Glarum, T. T. M. Palstra, A. R. Ramirez and A. R. Kortan, *Nature*, 1991, **350**, 600–601.
7 A. Y. Ganin, Y. Takabayashi, Y. Z. Khimyak, S. Margadonna, A. Tamai, M. J. Rosseinsky and K. Prassides, *Nat. Mater.*, 2008, **7**, 367–371.
8 D. Jérome, A. Mazaud, M. Ribault and K. Bechgaard, *J. Phys. Lett.*, 1980, **41**, L95–L98.
9 H. Taniguchi, M. Miyashita, K. Uchiyama, K. Satoh, N. Môri, H. Okamoto, K. Miyagawa, K. Kanoda, M. Hedo and Y. Uwatoko, *J. Phys. Soc. Jpn.*, 2003, **72**, 468–471.
10 R. Mitsuhashi, Y. Suzuki, Y. Yamanari, H. Mitamura, T. Kambe, N. Ikeda, H. Okamoto, A. Fujiwara, M. Yamaji,

N. Kawasaki, Y. Maniwa and Y. Kubozono, *Nature*, 2010, **464**, 76–79.
11 Y. Kubozono, M. Mitamura, X. Lee, X. He, Y. Yamanari, Y. Takahashi, Y. Suzuki, Y. Kaji, R. Eguchi, K. Akaike, T. Kambe, H. Okamoto, A. Fujiwara, T. Kato, T. Kosugi and H. Aoki, *Phys. Chem. Chem. Phys.*, 2011, **13**, 16476–16493.
12 X. F. Wang, R. H. Liu, Z. Gui, Y. L. Xie, Y. J. Yan, J. J. Ying, X. G. Luo and X. H. Chen, *Nat. Commun.*, 2011, **2**, 507.
13 M. Q. Xue, T. B. Cao, D. M. Wang, Y. Wu, H. X. Yang, X. L. Dong, J. B. He, F. W. Li and G. F. Chen, *Sci. Rep.*, 2012, **2**, 389.
14 Y. Kubozono, H. Goto, T. Jabuchi, T. Yokoya, T. Kambe, Y. Sakai, M. Izumi, L. Zheng, S. Hamao, H. L. T. Nguyen, M. Sakata, T. Kagayama and K. Shimizu, *Phys. C*, 2015, **514**, 199–205.
15 G. A. Artioli, F. Hammerath, M. C. Mozzati, P. Carretta, F. Corana, B. Mannucci, S. Margadonna and L. Malavasi, *Chem. Commun.*, 2015, **51**, 1092–1095.
16 Y. Gao, R.-S. Wang, X.-L. Wu, J. Cheng, T.-G. Deng, X.-W. Yan and Z.-B. Huang, *Acta Phys. Sin.*, 2016, **65**, 077402.
17 R.-S. Wang, Y. Gao, Z.-B. Huang and X.-J. Chen, 2017, arXiv:1703.05803.
18 R.-S. Wang, Y. Gao, Z.-B. Huang and X.-J. Chen, 2017, arXiv:1703.05804.
19 R.-S. Wang, Y. Gao, Z.-B. Huang and X.-J. Chen, 2017, arXiv:1703.06641.
20 P. Neha, V. Sahu and S. Patnaik, 2017, arXiv:1712.01766.
21 W. Liu, H. Lin, R. Kang, X. Zhu, Y. Zhang, S. Zheng and H.-H. Wen, *Phys. Rev. B*, 2017, **96**, 224501.
22 J.-F. Yan, R.-S. Wang, K. Zhang and X.-J. Chen, 2018, arXiv:1801.08220.
23 G. Huang, R.-S. Wang and X.-J. Chen, 2018, arXiv:1801.06324.
24 S. N. Putilin, E. V. Antipov and M. Marezio, *Phys. C*, 1993, **212**, 266.
25 G. H. Zhong, X. J. Chen and H. Q. Lin, 2015, arXiv:1501.00240.
26 K. Zhang, R.-S. Wang, A.-J. Qin and X.-J. Chen, 2018, arXiv:1801.06320.
27 R.-S. Wang, J. Cheng, X.-L. Wu, H. Yang, X.-J. Chen, Y. Gao and Z.-B. Huang, 2018, arXiv:1802.03320.
28 M. Casula, M. Calandra, G. Profeta and F. Mauri, *Phys. Rev. Lett.*, 2011, **107**, 137006.
29 G.-H. Zhong, C. Zhang, X. Yan, X. Li, Z. Du, G. Jing and C. Ma, *Mol. Phys.*, 2017, **115**, 472–483.
30 G.-H. Zhong, C.-L. Yang, X.-J. Chen and H.-Q. Lin, *J. Phys.: Condens. Matter*, 2018, **30**, 245703.
31 P. Durand, G. R. Darling, Y. Dubitsky, A. Zaopo and M. J. Rosseinsky, *Nat. Mater.*, 2003, **2**, 605–610.
32 Y. Takabayashi, A. Y. Ganin, P. Jeglič, D. Arčon, T. Takano, Y. Iwasa, Y. Ohishi, M. Takata, N. Takeshita, K. Prassides and M. J. Rosseinsky, *Science*, 2009, **323**, 1585–1590.
33 M. Kim, B. I. Min, G. Lee, H. J. Kwon, Y. M. Rhee and J. H. Shim, *Phys. Rev. B: Condens. Matter Mater. Phys.*, 2011, **83**, 214510.
34 G. Giovannetti and M. Capone, *Phys. Rev. B: Condens. Matter Mater. Phys.*, 2011, **83**, 134508.
35 A. Ruff, M. Sing, R. Claessen, H. Lee, M. Tomić, H. O. Jeschke and R. Valentí, *Phys. Rev. Lett.*, 2013, **110**, 216403.
36 G.-H. Zhong, C. Zhang, G.-F. Wu, Z.-B. Huang, X.-J. Chen and H.-Q. Lin, *J. Appl. Phys.*, 2013, **113**, 17E131.
37 G. Zhong, Z. Huang and H. Lin, *IEEE Trans. Magn.*, 2014, **50**, 1700103.
38 H. Li, X. Zhou, S. Parham, T. Nummy, J. Griffith, K. Gordon, E. L. Chronister and D. S. Dessau, 2017, arXiv:1704.04230.
39 M. Q. Ren, W. Chen, Q. Liu, C. Chen, Y. J. Qiao, Y. J. Chen, G. Zhou, T. Zhang, Y. J. Yan and D. L. Feng, 2017, arXiv:1705.09901.
40 T. Atake and H. Chihara, *Solid State Commun.*, 1980, **35**, 131–134.
41 G. Kresse and J. Furthmuller, *Comput. Mater. Sci.*, 1996, **6**, 15–50.
42 G. Kresse and J. Furthmuller, *Phys. Rev. B: Condens. Matter Mater. Phys.*, 1996, **54**, 11169–11186.
43 J. P. Perdew, K. Burke and M. Ernzerhof, *Phys. Rev. Lett.*, 1996, **77**, 3865.
44 K. Lee, E. D. Murray, L. Kong, B. I. Lundqvist and D. C. Langreth, *Phys. Rev. B: Condens. Matter Mater. Phys.*, 2010, **82**, 081101(R).
45 X. Wang, G. Zhong, X. Yan, X. Chen and H. Lin, *J. Phys. Chem. Solids*, 2017, **104**, 56–61.
46 M. Zhou, K. Wang, Z. Men, S. Gao, Z. Li and C. Sun, *Spectrochim. Acta, Part A*, 2012, **97**, 526–531.
47 K. Zhang and X.-J. Chen, *Spectrochim. Acta, Part A*, 2019, **206**, 202–206.
48 J. L. Bredas and G. B. Street, *Acc. Chem. Res.*, 1985, **18**, 309–315.
49 M. Dubois, G. Froyer, G. Louarn and D. Billaud, *Spectrochim. Acta, Part A*, 2003, **59**, 1849.
50 Y. Furukawa, H. Ohtsuka and M. Tasumi, *Synth. Met.*, 1993, **55**, 516–523.
51 G.-P. Charbonneau and Y. Delugeard, *Acta Crystallogr., Sect. B: Struct. Crystallogr. Cryst. Chem.*, 1976, **32**, 1420–1423.
52 G.-H. Zhong, C. Zhang, M. Chen, X.-J. Chen and H.-Q. Lin, *IEEE Trans. Magn.*, 2018, **54**, 7002105.